Compression-induced Ductile Flow of Brittle Materials and Brittle Fracturing of Ductile Materials

S. NEMAT-NASSER

Center of Excellence for Advanced Materials, Department of Applied Mechanics and Engineering Sciences, University of California, San Diego, La Jolla, CA 92093, USA

ABSTRACT

Even under all-around compressive loading, brittle materials tend to fail by the formation of tensile microcracks at microdefects such as cavities, grain boundaries, inclusions, and other inhomogeneities. As the overall confining pressure is increased, plastic flow tends to accompany microcracking, and eventually becomes the dominant mechanism of the overall deformation. Hence, under great confining pressure, brittle materials such as rocks can undergo large plastic flows before rupture.

A most remarkable phenomenon, recently predicted analytically and verified experimentally, is that a very ductile material, such as pure copper or mild steel, when deformed inhomogeneously plastically in compression, can develop extensive tensile cracks normal to the applied compression and in the absence of any overall tensile loads.

The article addresses the micromechanics of ductile flow of brittle materials and tensile fracturing of ductile materials under a broad range of compressive loads.

KEYWORDS

Compression, brittle-ductile transition, void collapse

1. INTRODUCTION

Whereas failure of materials and structural elements by formation and growth of tension cracks under *tensile* loading has been excessively studied and to a large extent understood, failure under overall compression has received considerably less attention. Historically, experimental investigation of compressive failure of materials such as rocks has often led to paradoxes. For example, Bridgman (1931) studied and demonstrated several failure modes peculiar to high pressures, leading to paradoxical results which impelled

him to express skepticism on whether there is such a thing as a genuine rupture criterion. The common feature of these paradoxes is that failure always occurs by the formation of *tension* cracks in specimens subjected to pure *compression*. Efforts to observe through electron microscopy the fracture pattern in failed specimens have raised further questions, since microcracks have been seen to have emanated from a variety of defects in various directions, although predominantly in the direction of maximum compression. These and related difficulties have led several authors to criticize micromechanical models that have been suggested for explaining brittle failure under compressive loads.

Over the past few years, several major developments have helped to bring the issue "brittle failure in compression" to a satisfactory level of basic understanding. The unexplained Bridgman paradox has been resolved (Scholz *et al.*, 1986), models which satisfactorily and quantitatively explain axial splitting, faulting, and transition from brittle to ductile modes of failure have been developed, and, most importantly, the mechanisms of fracturing in *loading* and *unloading* have been conclusively captured experimentally and by means of laboratory models. These have given considerable credence to the simple but very effective micromechanical modeling of brittle failure on the basis of preexisting flaws with frictional and cohesive resistance. Such a model can effectively capture the observed phenomenon of axial splitting in the absence of confinement, as well as the related phenomena of exfoliation or sheet fracture, and rockburst; Holzhausen (1978), and Nemat-Nasser and Horii (1982). In the presence of moderate confining pressures, furthermore, faulting by the interaction of preexisting microflaws has also been modeled by considering the interactive growth of tension cracks from an echelon of suitably oriented microflaws; Horii and Nemat-Nasser (1985). Furthermore, by including, in addition to tension cracks, possible zones of plastically deformed materials at the tips of preexisting flaws, the transition from brittle-type failure to ductile flow under very high confining pressures has been modeled; Horii and Nemat-Nasser (1986). A series of experimental model studies supports these analytical results. In particular, the influence of confining pressure on the mode of failure of brittle materials seems to have been clearly understood and modeled.

The above mentioned results are all for quasi-static loading and address microcracking during compressive loading: *the microcracks grow in the general direction of the maximum applied compression.*

During unloading, however, the microcracks are expected to grow essentially *normal* to the direction of the applied compression. This has been most vividly illustrated by a new set of dynamic experiments performed by the author and his co-workers at the University of California, San Diego. Indeed, it has been illustrated that, even extremely ductile crystalline solids such as single-crystal copper (an fcc metal), and mild steel and pure iron (bcc metals) can undergo *tensile cracking normal to the direction of compression*, possibly during the unloading phase under suitable conditions. In these tests the sample has never been subjected to any tension: only compressive loading and unloading. Nevertheless, tension cracks are developed basically *normal* to the applied compression.

In this paper we outline these findings, focusing on two main issues: (1) the mechanism of the ductile failure of brittle materials under large confining pressures; and (2) the mechanism of the apparently brittle failure of ductile materials under dynamic compressive loads. This second topic also bears on the proper post-mortem interpretation of compressively failed specimens, since it clearly demonstrates how tensile cracks are created

normal to the direction of compression, apparently during the unloading (removal of compression) of specimens which have never been subjected to any (overall) tensile forces.

2. FAILURE OF BRITTLE MATERIALS IN COMPRESSION

2.1 Bridgman Paradox

Bridgman performed experiments on failure in compression, which led to three paradoxes. In each case, a sample was subjected to high pressures by immersing it in a pressurized fluid. Two of Bridgman's paradoxes, one called "the pinching-off effect" and the other the "ring paradox," have already been resolved; see Jaeger and Cook (1963), and Scholz *et al.* (1986), where it is shown that tensile failure in an all-around compressive environment is basically due to "hydraulic fracturing." A third paradox, however, has been far more elusive and does indeed touch on some rather subtle aspects of *brittle failure of brittle materials under all-around compressive loads*. The corresponding experiment has been carefully repeated by Scholz *et al.* (1986), and then satisfactorily quantitatively explained in terms of model calculations of Nemat-Nasser and Horii (1982). The experiment consists of a thin cylindrical tube of pyrex glass, tightly fitted over a solid steel cylinder, and then carefully sealed. Then the composite is enclosed by a sealed membrane and subjected to all-around uniform confining pressure; Fig. 1a.

By direct measurement through strain gauges placed on the glass tube and by simple calculations, it is established that *all three principal stresses everywhere within the glass tube are compressive*. Nevertheless, it is observed that tension cracks develop from the interior surface of the glass tube in the radial direction, grow axially in a stable manner, and never reach the exterior surface of the tube.

The paradox has been explained by Scholz *et al.* (1986), by considering a preexisting flaw with suitable inclination, and by estimating the required flaw size which can produce tension cracks under the prevailing compressive stress state, in accordance with the "sliding crack model" initially proposed by Brace and Bombolakis (1963); Fig. 1b.

Fig. 1. (a) Bridgman experiment.

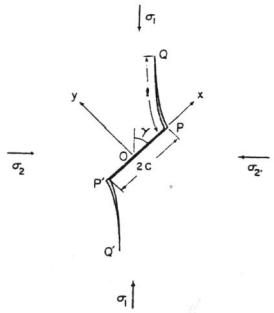

Fig. 1b. Preexisting flaw PP′ and curved tension cracks PQ and P′Q′.

Calculations based on the Nemat-Nasser and Horii (1982) theory show that a preexisting flaw size of 10 μm is sufficient to produce such axial tension cracks. SEM observations showed that all axial cracks emanated from preexisting flaws of about 20 μm, and that the axial cracks consisted of several individual cracks which seem to have been initiated from different preexisting flaws.

This is perhaps the most conclusive laboratory experiment which not only resolves the Bridgman paradox, but also shows the role of preexisting flaws in generating tensile cracks under all-around compression in brittle solids. The fact that flaws in the pyrex glass of this experiment are few and far apart, precludes their interaction, leading to only axial cracking. In a rock, ceramic, or similar specimen, there are numerous preexisting microflaws such as pores, grain boundaries, preexisting cracks, and inclusions, each of which can be and often is a source of producing local tensile stresses, even though the farfield applied loads may all be compressive.

2.2 A New Look at Microcracking in Compression

The fact that *axial splitting* under uniaxial compression is caused essentially by nucleation at various flaws of tension cracks which grow essentially in the direction of compression, has been most vividly demonstrated in a recent series of experiments by Professor Cook and his associates at the University of California, Berkeley (Ziqiong Zheng *et al.*, 1988). In these experiments the microstructure of the compressed sample is preserved by impregnating the specimen with molten Wood's metal which solidifies prior to the removal of the compressive loads. The sample is then sectioned and studied. The presence of the solidified alloy which penetrates tube-like pores of diameters exceeding 0.16μm, and planar cavities with apertures exceeding 0.08μm, does not allow further fracturing during unloading. Hence, microcracking produced solely during the application of compression can be studied. The authors conclude that a variety of microscopic mechanisms (sliding, point loading, and bending) produce tensile cracking parallel to the direction of maximum compression.

2.3 Model Experiments

The model experiments by Brace and Bombolakis (1963), Hoek and Bieniawski (1965), and Nemat-Nasser and Horii (1982), yield similar results. In addition, Horii and Nemat-Nasser (1985, 1986) have provided clear illustration of transition from the axial splitting mode of failure to faulting, when axial compression is applied in the presence of lateral confinement, and the transition from a brittle to a ductile mode of failure, when the confining pressure is suitably large.

The experiments involve thin plates of relatively brittle material (e.g., Columbia resin CR39) containing thin slits (flaws) fitted with thin brass sheets, and subjected to in-plane compression. Tension cracks similar to those shown in Fig. 1b, nucleate from the flaws, curve toward the direction of maximum in-plane compression and grow with increasing compression, becoming eventually parallel to this loading direction. Of particular interest in these experiments is the fact that the presence of slight in-plane lateral tension can render a crack growth regime of this kind unstable: once a critical crack extension length is attained, the crack would grow spontaneously, leading to axial splitting of the specimen. Nemat-Nasser and Horii seek to explain the phenomena of axial splitting, exfoliation or sheet fracture (Holzhausen, 1978), and rockburst, using this observation.

It therefore appears that, in the absence of lateral confinement, axial splitting may well be the result of the formation of axially oriented tension cracks at the tips of the existing most compliant inhomogeneities. These cracks then grow axially and lead to axial splitting. Once such a process is initiated, the specimen no longer remains homogeneous in a continuum sense. At this stage the strength drops dramatically. Figure 2 shows a model experiment of this phenomenon.

When lateral confinement accompanies axial compression, a dramatic change in the overall response of rocks, concrete, ceramics, and other brittle materials is often observed. Microscopic observation shows that, in this case also, microcracks are nucleated at various micro-inhomogeneities, and these cracks grow essentially in the direction of maximum compression. However, the presence of confinement seems to arrest further growth of cracks of this kind. Indeed, electron microscopy, as well as optical microscopy, seem to suggest a more or less uniform distribution of microcracks within the sample, up to axial loads rather close to the peak stress; see, for example, Hallbauer, Wagner, and Cook (1973), Olsson and Peng (1976), and Wong (1982). Close to the peak stress a region of high-density microcracks begins to emerge, which eventually becomes the final failure plane. The sample fails by faulting at an angle somewhere between 10 and 30° with respect to the axial compression.

Nemat-Nasser and Horii (1985, 1986) have suggested that such faulting may be the result of the interactive unstable growth of tension cracks at the tips of suitably oriented sets of microflaws. To verify this, a series of model experiments are made on plates which contain sets of small flaws and a number of large flaws; a flaw here is a thin slit (0.4 mm thick) containing two thin brass sheets (0.2 mm each). Two identical specimens are tested, one without confining pressure, the other with some confinement; see Fig. 3. In the absence of confinement, cracks emanate from the tips of the longer flaws, grow in the direction of axial compression, and lead to axial splitting, while many of the smaller flaws have not even nucleated any

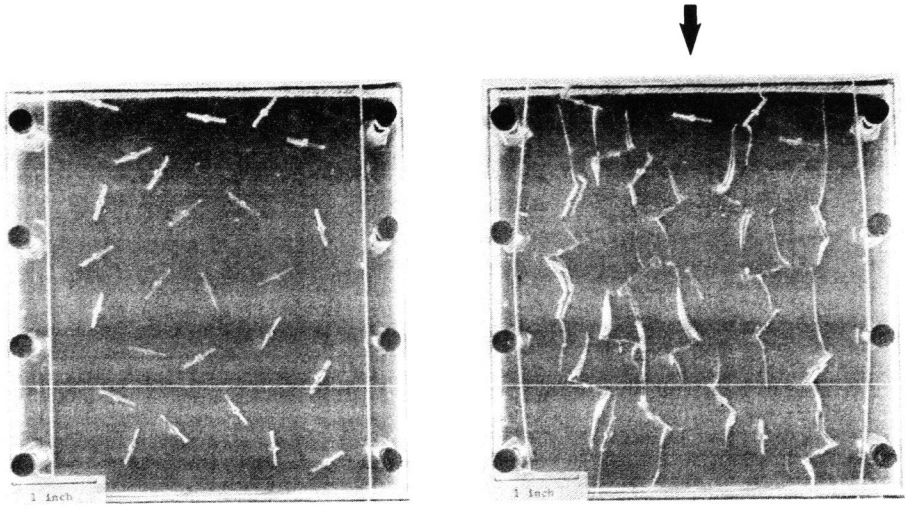

(a) (b)

Fig. 2. (a) Specimen with a number of randomly oriented cracks, and (b) the failure pattern under overall axial compression (from Nemat-Nasser and Horii, 1982).

cracks, Fig. 3b. On the other hand, when some confinement accompanies axial compression, cracks emanating from the larger flaws are soon arrested. Then, at a certain stage of loading, suddenly, cracks emanating from many small flaws grow in an unstable manner, leading to eventual faulting; Fig. 3c.

When the confining pressure is quite large, e.g. exceeding 25-30% of the peak stress, then a transition from brittle failure by faulting to the ductile response by overall plastic flow takes place. Microscopic observation shows a rather general distribution of microcracks accompanying extensive plastic deformation. (These are at suitably low temperatures, where creep effects can be regarded insignificant.) The sample may fail by either localized plastic shearing or by barreling. Horii and Nemat-Nasser (1986) suggest a model which seems to illustrate the involved mechanism.

Figure 4 shows a sample containing two collinear flaws. When in-plane axial compression is applied in the presence of relatively large confining pressures, both tension cracks and plastically deformed zones develop close to the tip of the preexisting flaws. That is, under axial compression, cracks can emanate from the tips of the flaw, while at the same time plastic zones can grow there. The crack length and the size of the plastic zone depend on the confining pressure. For moderate confinement, the tension crack length increases at a great rate, while the plastic zone size remains limited. On the other hand, once suitable confinement exists, the tension crack soon ceases to grow in response to the increasing axial compression, while the plastic zone size continues to increase. Indeed, if the confinement is large enough, the growth of the plastic zone may, at a

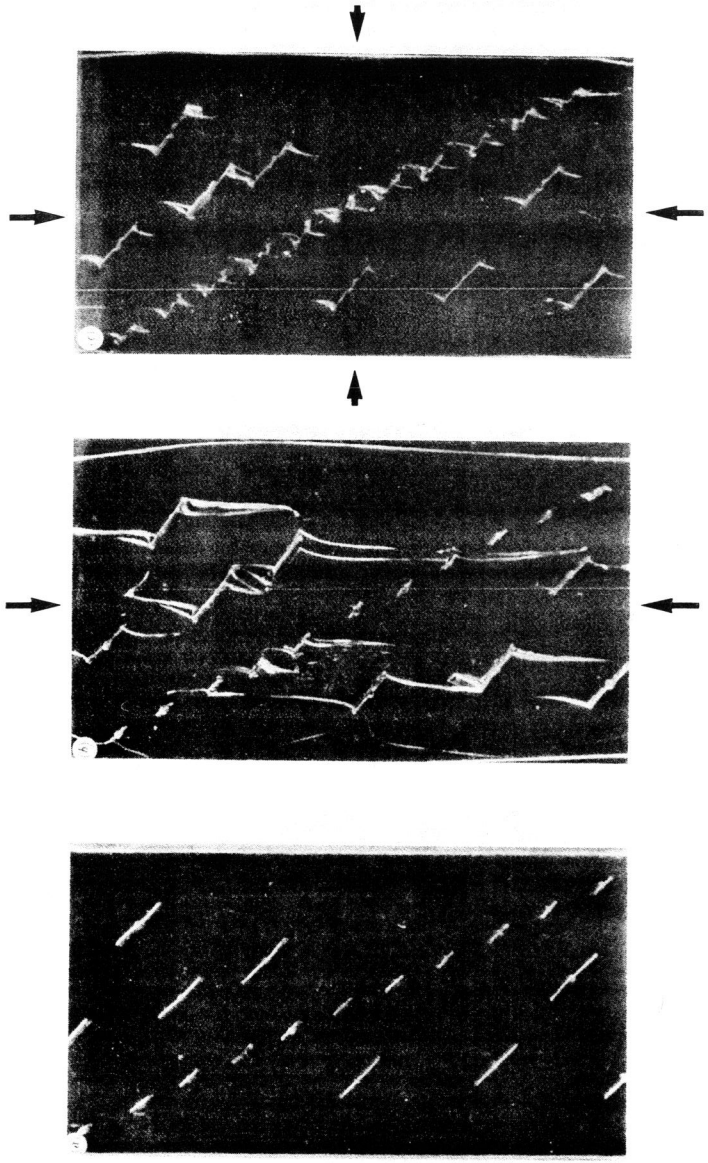

Fig. 3. (a) Specimen containing a row of small flaws and several larger flaws. (b) Axial splitting under axial compression *without* lateral confinement; (c) shear failure under axial compression *with* lateral con-finement (from Horii and Nemat-Nasser, 1985).

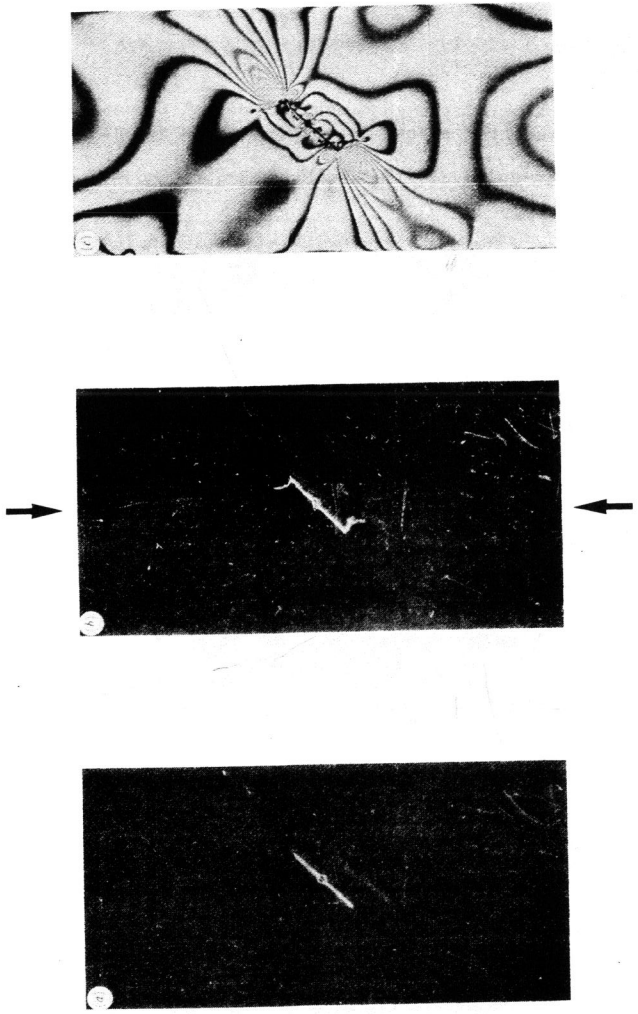

Fig. 4. (a) A specimen with two collinear flaws. (b) Arrested tension cracks emanating from the ends of the flaws under axial and lateral compressive stresses of constant ratio $\sigma_2/\sigma_1 = 0.05$. (c) Photoelastic picture of the unloaded specimen showing the residual strain distribution (from Horii and Nemat-Nasser, 1985).

certain stage, actually relax the stress field around the tension crack, resulting in partial closure of the tension crack. Based on this model, Horii and Nemat-Nasser (1986) estimate the brittle-ductile transition pressure, and obtain results in close correlation with experimentally observed values.

2.4 Model Calculations

2.4.1 Axial Splitting. The two-dimensional elasticity boundary value problem associated with the model shown in Fig. 1b has been formulated in terms of singular integral equations and solved, using an effective numerical technique; Nemat-Nasser and Horii (1982) and Horii and Nemat-Nasser (1983). The boundary conditions on the flaw PP′ are

$$u_y^+ = u_y^-, \quad \tau_{xy}^+ = \tau_{xy}^- = -\tau_c + \mu\sigma_y \ , \tag{1}$$

and on the curved cracks PQ and P′Q′, one requires

$$\sigma_\theta = \tau_{r\theta} = 0 \ , \tag{2}$$

where τ_c is the cohesive (or yield) stress, μ is the frictional coefficient, u_y is the displacement in the y-direction, σ_y is the normal stress and τ_{xy} is the shear stress on PP′, and σ_θ is the hoop stress and $\tau_{r\theta}$ is the shear stress on PQ. Superscripts + and - denote the values of the considered quantities above and below the x-axis. Figure 5 shows some typical results.

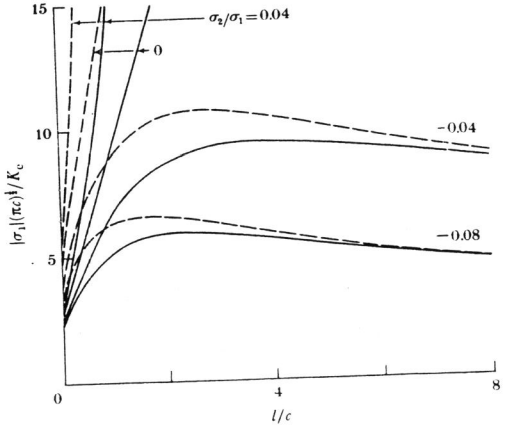

Fig. 5. Normalized axial compression required to attain the associated crack extension length (from Horii and Nemat-Nasser, 1983).

As is seen, in the presence of small lateral tension, crack growth becomes unstable after a certain crack extension length is attained. This unstable

crack growth is considered to be the fundamental mechanism of axial splitting of a uniaxially compressed rock specimen. Peng and Johnson (1972) report the presence of lateral tension in the uniaxially compressed specimen because of the end-boundary conditions. Different end inserts affect the ultimate strength. They report a radial tensile stress of 4-8% of the applied compression. These experimental data seem to support the analytical results.

Nemat-Nasser and Horii (1982) have made a series of model experiments and have shown that unstable growth of tension cracks discussed above, may indeed be the basic micromechanism of axial splitting; see their Figs. 13-20.

The numerical calculations of the singular integral equation which corresponds to the elasticity model of Fig. 1b are rather laborious. Furthermore, they preclude further modeling which often requires simple closed-form analytic expressions. Efforts have been made to develop such expressions for the model of Fig. 1b, by substituting for the curved cracks equivalent straight cracks; see, e.g. Ashby and Cookley (1986), Steif (1984), and Horii and Nemat-Nasser (1986). Among these, the last authors have given simple but very effective expressions which seem to yield accurate results over the entire range of crack lengths and orientations. Indeed, in a more recent article, Nemat-Nasser and Obata (1988) have used these analytical expressions to model the dilatancy and the hysteretic cycle observed in rocks. We briefly outline the analytical solution of Horii and Nemat-Nasser (1986).

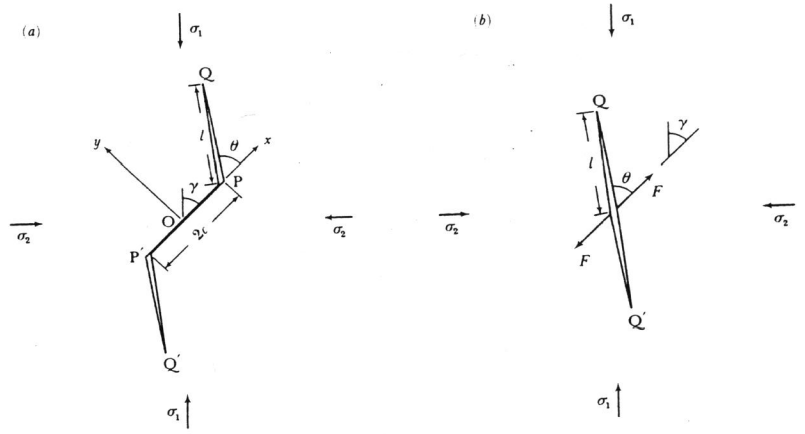

Fig. 6. (a) Preexisting flaw PP′ and straight cracks PQ and P′Q′. (b) a representative tension crack QQ′ with splitting forces F.

Figure 6a shows the flaw with straight cracks, and Fig. 6b shows a crack of length 2ℓ subjected to a pair of forces of common magnitude F which represents the effect of the flaw on cracks PQ and P′Q′. These cracks are additionally subjected to farfield stresses σ_1 and σ_2. The force F is

estimated from the driving shear stress τ^*, on the preexisting flaw,

$$F = 2c\tau^* , \tag{3}$$

$$\tau^* = -\tfrac{1}{2}(\sigma_1 - \sigma_2)\sin 2\gamma - \tau_c + \tfrac{1}{2}\mu[\sigma_1 + \sigma_2 - (\sigma_1 - \sigma_2)\cos 2\gamma] .$$

Then, under the action of the concentrated coaxial forces of magnitude F and the farfield streses, the stress intensity factors are given by

$$K_I = 2c\tau^* \sin\theta/\{\pi(\ell+\ell^*)\}^{1/2} + (\pi\ell)^{1/2}\tfrac{1}{2}[\sigma_1+\sigma_2-(\sigma_1-\sigma_2)\cos 2(\theta-\gamma)] , \tag{4}$$

$$K_{II} = -2c\tau^* \cos\theta/\{\pi(\ell+\ell^*)\}^{1/2} - (\pi\ell)\}^{1/2}\tfrac{1}{2}(\sigma_1-\sigma_2)\sin 2(\theta-\gamma) .$$

In this equation, $\ell^*/c = 0.27$ is introduced so that when the crack length ℓ is vanishingly small, the corresponding stress intensity factors are still accurately given by Eqs. (4). Note that, when ℓ is large, the presence of ℓ^* is of little consequence. Thus, Eqs. (4) are good estimates over the entire range of crack lengths.

2.4.2 Faulting. In the presence of confining pressure, an axially compressed sample of rock fails by faulting or (macroscopic) shear failure. To explain the mechanics of such faulting, some authors have emphasized the role of Euler-type buckling associated with columnar regions formed in the sample because of axial cracking; see, for example, Fairhurst and Cook (1966), Janach (1977), and Holzhausen and Johnson (1979).

A different model has been suggested by Horii and Nemat-Nasser (1983, 1985). This model considers a row of suitably oriented microflaws and seeks to estimate the axial compression at which out-of-plane cracks that nucleate from the tips of these flaws can suddenly grow in an unstable manner, leading to the formation of a fault; see Fig. 7.

The solution of the elasticity problem associated with a solid containing a row of periodically distributed flaws with out-of-plane microcracks, is given by Horii and Nemat-Nasser (1983, 1985). Typical results are shown in Fig. 8.

For small values of ϕ, the axial compression first increases with increasing crack extension length, attains a peak value, decreases, and then begins to rise again. This suggests an unstable crack growth at a critical value of the axial stress, which may lead to the formation of a fault zone. It is seen from Fig. 8 that the peak values of the axial stress for the values of ϕ from 0.16π to 0.2π fall in a very narrow range, i.e. $|\Delta\sigma_1|\sqrt{\pi c}/K_c \simeq 0.3$. This implies that the overall failure angle is sensitive to imperfection and other effects. Indeed, the orientation of the fracture plane observed in experiments often scatters over a certain range. The range of the overall failure angle, however, may be limited since the peak value of the axial stress increases sharply as ϕ decreases. We can specify the possible range of the overall orientation angle ϕ by prescribing the "stress barrier" $|\Delta\sigma_1|\sqrt{\pi c}/K_c$ which can be overcome. Note that the value of γ in Fig. 7 is chosen such that the required axial compression for instability is minimized.

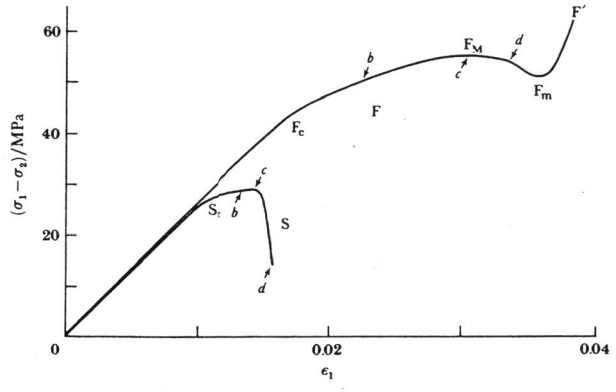

Fig. 7. An unbounded two-dimensional solid with a row of preexisting flaws PP′ and tension cracks PQ and P′Q′.

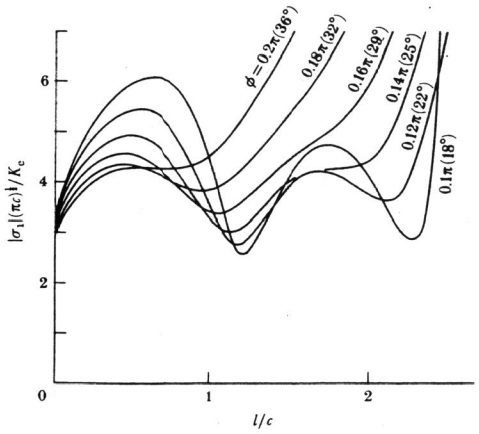

Fig. 8. Axial stress versus crack extension length: $\gamma = 0.24\pi$, $\tau_c = 0$, and $\mu = 0.4$ (from Horii and Nemat-Nasser, 1983).

2.4.3 Brittle-ductile transition. Brittle failure by faulting is suppressed by sufficiently high confining pressures that promote more or less uniformly distributed inelastic deformation throughout the sample. Microscopically, however, the deformation remains highly heterogeneous, in view of the microstructure of the material. Depending on the material and the

temperature, the inelastic deformation may stem from grain-size microcracking, plastic glide, or a combination of the two. For example, in marble and limestone, as well as in pyroxenes, microcracking and the associated cataclastic flow can be inhibited at room temperature by large enough confining pressures, whereas for other materials, such as quartz and feldspar, this requires higher temperatures (Donath *et al.*, 1971; Tobin and Donath, 1971; Olsson and Peng, 1976; Tullis and Yund, 1977; Kirby and Kronenberg, 1984). It is instructive to examine the influence of increasing lateral pressure on the interactive, unstable crack growth associated with a row of preexisting flaws, shown in Fig. 7. For $\phi = 29°$, $\gamma = 43°$, and $d/c = 4$, the results are shown in Fig. 9. It is seen that increasing the lateral pressure suppresses the unstable growth of tension cracks emanating from the tips of the interacting flaws, and therefore the associated faulting.

To estimate analytically the brittle-ductile transition, Horii and Nemat-Nasser consider the model shown in Fig. 10.

It consists of the frictional and cohesive flaw PP′ which has produced, at its tips, out-of-plane tension cracks PQ and P′Q′ of common length ℓ_p. The boundary conditions on the preexisting flaw and the tension cracks are given, respectively, by (1) and (2). The conditions on the slip lines PR and P′R′ are

$$u_y^+ = u_y^-, \quad \tau_{xy} = -\tau_Y \ , \tag{5}$$

where τ_Y is the yield stress in shear. The principal stresses at infinity are prescribed to be σ_1 and σ_2. In this model the tension cracks are assumed to be straight. The plastic zones are modeled by dislocation lines collinear with the preexisting flaw, as motivated by the model experiments, although it is not difficult to consider a non-collinear dislocation line or several such lines, depending on the circumstances. The use of collinear dislocation lines is reasonable and seems to yield adequate results.

The stresses at the ends of the plastic zones must be bounded. We seek a solution that renders the Mode II stress intensity factor at R and R′ zero, i.e. we require

$$K_{II}^R = 0, \text{ at R and R}' \ . \tag{6}$$

Horii and Nemat-Nasser (1986) present exact formulation and solutions for the problem sketched in Fig. 10, in terms of singular integral equations. They also give approximate closed form solutions which may prove more effective for further modeling. The approximate analytical solution is based on assumptions that the ductility defined by the following parameter:

$$\Delta = K_c/[\tau_Y\ (\pi c)^{1/2}] \tag{7}$$

is small, and the size of the tension crack is large relative to the size of the plastic zone. Hence, the interaction between the plastic zone and the crack is neglected. The stress intensity factor K_I at Q and Q′ is estimated using Eq. (4). Then the Dugdale (Dugdale, 1960) model is used in Mode II to estimate the size of the plastic zone such that $K_{II}^R = 0$ at points R and R′ in Fig. 10. This yields the following expression for σ_1/τ_Y :

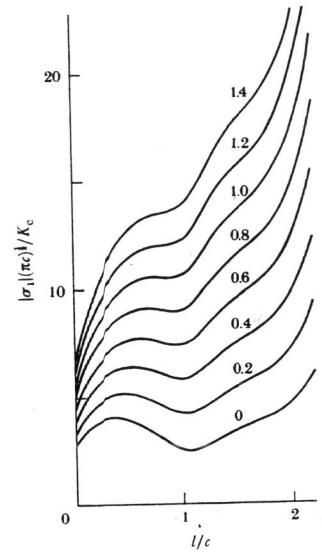

Fig. 9. Compressive force required to attain the associated length of cracks enamating from a row of preexisting flaws, under the indicated normalized lateral stresses (contours of $|\sigma_2|(\pi c)^{1/2}/K_c$), with d/c = 4, γ = 43° and ϕ = 29° (from Horii and Nemat-Nasser, 1986).

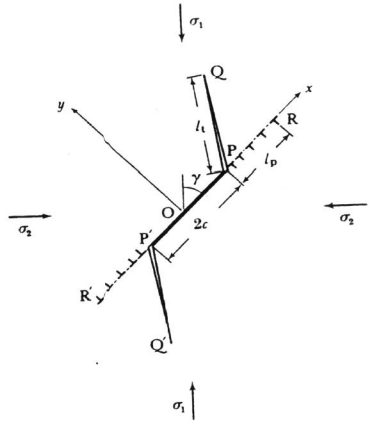

Fig. 10. Preexisting flaw PP', tension cracks PQ and P'Q', and plastic zones PR and P'R'.

$$(-\sigma_1)/\tau_Y = \left[2+\frac{4}{\pi}(\tau_c/\tau_Y-1)\arcsin\left(\frac{1}{1+\ell_p/c}\right)\right]/ \tag{8}$$

$$\left\{(1-\sigma_2/\sigma_1)\sin 2\gamma-\mu[1+\sigma_2/\sigma_1-(1-\sigma_2/\sigma_1)\cos 2\gamma]\frac{2}{\pi}\arcsin\left(\frac{1}{1+\ell_p/c}\right)\right\},$$

and in view of (4) we obtain

$$\frac{K_I}{\tau_Y(\pi c)^{1/2}} = \frac{\sin\theta}{\pi(\ell_t/c+\ell_t^*/c)^{1/2}}\left\{\frac{-\sigma_1}{\tau_Y}[(1-\sigma_2/\sigma_1)\sin 2\gamma \right. \tag{9}$$

$$\left. -\mu(1+\sigma_2/\sigma_1-(1-\sigma_2/\sigma_1)\cos 2\gamma)]-\frac{\tau_c}{\tau_Y}\right\}$$

$$-(\ell_t/c)^{1/2}\frac{(-\sigma_1)}{\tau_Y}\tfrac{1}{2}[1+\sigma_2/\sigma_1-(1-\sigma_2/\sigma_1)\cos 2(\theta-\gamma)] .$$

Horii and Nemat-Nasser (1986) examine the accuracy of (8) and (9) by comparing the corresponding results with the numerical ones for the exact formulation. For ductility Δ less than about 0.1 the approximate results are quite good. One shortcoming of the approximate results (8) and (9) is that they do not yield a maximum value for the size of the tension cracks, whereas the exact calculation does. Figure 11 shows the relation between ℓ_t/c and ℓ_p/c for Δ = 0.04 and Δ = 0.08, obtained by the numerical solution of the singular integral equations for the exact formulation of the boundary-value problem.

From the results presented in Fig. 11, it is seen that for small lateral compression, ℓ_p/c remains very small as ℓ_t/c increases; the response of the solid is "brittle" in this case. With suitably large values of σ_2/σ_1, on the other hand, ℓ_t/c ceases to increase after it attains a certain value, while ℓ_p/c continues to increase with increasing axial compression. Indeed, for large enough σ_2/σ_1 (e.g. σ_2/σ_1 = 0.2), the tension crack actually begins to relax and close as the plastic zone extends. Horii and Nemat-Nasser suggest that this may be the fundamental mechanism responsible for the brittle-ductile transition. In fact, if the peak values of ℓ_t/c (denoted by $(\ell_t/c)_{max}$) are plotted against σ_2/σ_1, Fig. 12 is obtained.

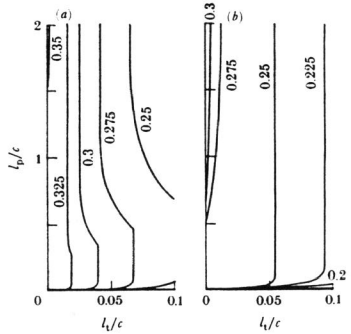

Fig. 11. Relation between the tension crack length and the size of the plastic zone under proportional loading for indicated stress ratios (contours of σ_2/σ_1), for (a) Δ = 0.04 and (b) Δ = 0.08 (from Horii and Nemat-Nasser, 1986).

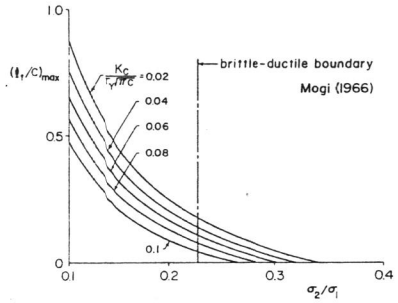

Fig. 12. The maximum length of tension cracks as a function of stress ratio (from Nemat-Nasser and Horii, 1984).

For σ_2/σ_1 exceeding 0.2 to 0.25, this figure shows a transition to the ductile response. This is in accord with experimental observations; Mogi (1966). We note from Fig. 11 that, for σ_2/σ_1 greater than certain values, the size of the plastic zone continues to grow with increasing compression (for proportional loading), once ℓ_t/c attains certain maximum values. A deformation process of this kind characterizes the 'ductile mode'. The change from brittle to ductile mode is illustrated in Fig. 11a,b for Δ = 0.04 and 0.08 respectively. It is seen that this change occurs when the stress ratio increases from 0.325 to 0.35 for Δ = 0.04, and from 0.25 to 0.275 for Δ = 0.08.

It is seen that whether the failure is brittle, being dominated by the growth of tension cracks, or ductile, being dominated by the growth of plastic zones, depends on the magnitude of the stress ratio, σ_2/σ_1, and the overall ductility, Δ. The influence of temperature enters implicitly through the associated values of fracture toughness, K_c, and yield stress, τ_Y. Since the former increases and the latter decreases with increasing temperature, Δ increases with increasing temperature. It is shown by Horii and Nemat-Nasser (1986) that when Δ is suitably large, the growth of tension cracks can be essentially suppressed by suitable confinement. For a Δ of the order of a few percent, however, both tension cracks and plastic deformation can occur. The material for a small Δ is inherently "brittle". However, suitably large confining pressures suppress unstable growth of microcracks and promote plastic flow instead. Hence, compression can induce plastic flow of crystalline solids which are commonly classified as "brittle".

3. FAILURE OF DUCTILE MATERIALS IN COMPRESSION

As discussed in the preceding section, the main characteristic of the failure of *brittle* materials in compression is the formation of microcracks predominantly in the direction of maximum compression. One of the most interesting recent discoveries is that ductile materials such as copper, mild steel, and iron, can fail in compression by the formation of *tensile* cracks normal to the direction of the applied compression. The phenomenon is highly rate-dependent and requires heterogeneous large plastic deformations to precede the *removal* of the compressive stresses. It is believed that the cracking occurs during the unloading, and a number of experiments by the author and co-workers seem to support this conjecture.

The possibility of tensile cracks developing in an fcc single crystal during the removal of compression, was brought into focus by micromechanical calculations of Nemat-Nasser and Hori (1987) who used a rate-dependent slip-induced plasticity theory to calculate void growth and void collapse in single crystals. Assuming that the response of the solid during unloading is essentially elastic, these authors examine possible tensile cracking from the tips of a collapsed void in a single crystal. The calculation shows that indeed, tensile cracking can take place during unloading in a specimen which has been subjected to only overall compressive forces.

3.1 Computational Results

The computation of void collapse (or growth) by Nemat-Nasser and Hori (1987) is based on decomposing the total deformation rate tensor into an elastic part and a plastic part. The stress rate is expressed in terms of the elastic part of the deformation rate tensor, by Hooke's law. The rate of plastic slip of each slip system is assumed to be governed by a power-law, $\dot{\gamma}=\eta(\tau/\tau_r)^n$, where η, τ_r, and n are regarded as material parameters, and τ is the resolved shear stress. The exponent n is large, say, n = 100, for small strain rates, and is taken to be unity when the strain rate exceeds 10^4/s. The flow stress τ_r, in general, depends on the deformation history and includes the material hardening effects. In the actual analytical computations of Nemat-Nasser and Hori (1987), τ_r is assumed to remain constant. The solution is obtained incrementally, using a set of assumptions. For plane problems involving an initially circular void with radius a_r, the solution involves the following steps:

1) At a typical time t_0, an elliptical cavity in an infinite elastoplastic solid is considered. The stress field $\underset{\sim}{\sigma}(t_0)$ is known. The solid is then subjected to a farfield incremental loading defined by stress rate $\dot{\underset{\sim}{\sigma}}^{\infty}$.

2) The instantaneous response is assumed to be purely elastic for a step loading $\Delta\underset{\sim}{\sigma}^{\infty} = \dot{\underset{\sim}{\sigma}}^{\infty}\Delta t$, and the instantaneous stress rate $\dot{\underset{\sim}{\sigma}}(t_0)$ and the incremental stress field $\Delta\underset{\sim}{\sigma} = \dot{\underset{\sim}{\sigma}}(t_0)\Delta t$ are calculated. The new stress field $\underset{\sim}{\sigma}(t_0+\Delta t)$ is then obtained as the sum of $\underset{\sim}{\sigma}(t_0)$ and $\Delta\underset{\sim}{\sigma}(t_0)$, $\underset{\sim}{\sigma}(t_0+\Delta t) = \underset{\sim}{\sigma}(t_0) + \Delta\underset{\sim}{\sigma} + O(\Delta t^2)$.

3) From the current stress field, the resolved shear stress on each slip system is calculated, and the current plastic deformation rate and spin tensors are obtained. The corresponding displacement gradient is then obtained from the sum of the elastic and plastic parts.

4) Ignoring the elastic contribution to the void shape change, and taking a sufficiently small time increment, the incremental small displacements of the points along the void boundary are computed; this deformation by rate-dependent plastic flow is assumed to take place during the time increment Δt.

5) The new void geometry, in general, will not be elliptical. To continue the computation, an *equivalent* elliptical void is calculated, using the following criteria:

   a) The maximum distance from the center to the perimeter of the deformed void is taken to be the major semi-axis a_1 of the equivalent ellipse.
   b) The orientation which gives the maximum distance is taken to be the orientation of the major semi-axis.
   c) The aspect ratio of the equivalent ellipse is defined by $\rho=A/\pi a_1^2$, with

A being the actual area of the deformed void.

This procedure is continued until the aspect ratio of the equivalent ellipse is so small that the ellipse may be regarded to be a crack (void collapse), or until the aspect ratio attains a limiting value with the void area increasing in an unstable manner (self-similar expansion).

The analysis of possible tensile cracking is based on the simple assumptions that unloading occurs elastically and that the crack may grow if the Mode I stress intensity factor exceeds a given critical value. The Mode I stress intensity factor at the tip of a crack of length 2a (which is obtained by the extension of a crack of length $2a_1$ formed by a collapsed void), due to the superposition of accumulated stresses during loading and released stresses during unloading, is given by

$$K_I = \int_{a_1}^{a} \sigma_n^{(\ell)}(\zeta)\, 2\sqrt{a}\, \frac{d\zeta}{(\pi(a^2-\zeta^2))^{1/2}} + \sigma_n^{\infty(u)} \sqrt{\pi a}, \qquad (10)$$

where the subscript n denotes the stress component normal to the crack face, it is assumed that the crack faces remain traction-free, and that the far-field stresses existing prior to unloading are removed by the amount $\sigma_n^{\infty(u)}$. In (10), superscript ℓ on σ stands for the magnitude of the stress during loading, and superscript u stands for the unloading stress. In the actual calculation the extended crack length defined by a, is chosen such that the value of K_I, calculated from (10), equals the prescribed critical value of the stress intensity factor.

The calculation shows and experiment verifies that higher compressive loads are required at higher loading rates, in order to collapse a void. Hence, larger stress intensity factors are attained in complete unloading, when void collapse occurs at higher loading rates. Thus the response of the same material containing the same microvoids will not be the same when the loading rate is changed: the material becomes stronger but more brittle at higher (compressive) loading rates.

The process of void growth and void collapse and the subsequent failure mechanisms depend on the orientation of the slip systems, the state of stress, the rate of loading, and the initial void size. The following general results are obtained.

1) Even under all-around uniform compression, an initially spherical (circular in two dimensions) void quickly becomes nonshperical and may collapse into a crack. Depending on the rate of loading, the ductility of the material (which is also affected by the rate of loading), and the initial void size, the crack which is formed by the void collapse may extend in its own plane during the course of unloading, leading to failure by a brittle type tensile fracture, even though the material has not been subjected to any overall tensile loads. This occurs at high strain rates for sufficiently large voids. The minimum void size required for such a failure decreases with an increasing compressive loading rate.

2) Void collapse in compression and void growth in tension are basically different processes and one cannot be regarded as the reverse of the other. Thus, phenomenological models currently used to estimate ductile fracture, which do not distinguish between void growth and void collapse, are of limited usefulness.

3) An initially circular (in two dimensions) void may collapse into a crack,

even under uni-axial tension, if the orientations of the slip systems are suitable. Similarly, overall shear stresses can collapse a void into a crack. However, under tensile loads, voids usually expand into ellipsoidal cavities which may then grow self-similarly in an unstable manner, leading to ductile failure. Figure 13 gives typical results for void collapse in uni-axial compression, using a double-slip plane deformation assumption.

3.1 Experiments

In a series of experiments by the author and co-workers (Dr. Soon-Nam Chang and Mr. Jason Schwartz) it has been conclusively established that tension cracks normal to the direction of the applied compression can actually develop in both fcc and bcc metals when the plastic deformation preceding unloading is highly heterogeneous, and a suitable stress concentrator does exist.

The experiment involves collapse of a cylindrical void in a specimen under quasi-static or dynamic loads. Copper (single and polycrystal), 1018 mild steel, 4340 steel, and pure iron specimens have been used. The tests involve a small rectangular sample containing a small (120 to 600 μm) circular cylindrical cavity. Samples are supported against buckling by sandwiching them between semicircular cylindrical or other suitable pieces of the same material. The sandwiched assembly is held together in a steel annulus whose height is selected to limit the total compressive deformation to a predetermined amount of plastic strain. The assembly is held in the steel annulus with Styrofoam pillows. Supporting pieces (and specimens) are annealed when necessary. Records of hole shape are made before and after testing. Both quasi-static and dynamic (in a split Hopkinson bar) tests are performed.

Figure 14 shows the collapsed void in single-crystal copper axially strained by about 21.4% at a 1,100/s strain rate. The upper figure shows the collapsed void. The crystal is cut in such a manner that two slip systems in the plane of the specimen are activated. Hence, the thickness remains essentially constant. Since one of the slip systems dominates, the deformed void rotates, and the final configuration is not quite normal to the axis of compression. The two lower figures in Fig. 14 are the electronmicroscopic record of the polished and etched specimen. As is seen, the collapsed void has extended as a crack in dynamic crack growth fashion, resulting in multi-branching which suggests a rather high crack-growth velocity. Experiments of this kind clearly have shown that the cracks extend in many different directions and not only in the direction of the cleavage plane of the crystal.

Figure 15 shows void collapse (initial void size of about 600 μm) in compression, and subsequent crack growth in 1018 mild steel, at various indicated strain rates. Extensive crack branching is observed which is an indication of very high velocity crack growth. The tensile cracks initially run straight ahead for a distance and then branch out. The resistance of the material to plastic flow during compressive loading and the extent of subsequent tensile cracking decreases with decreasing strain rate; compare the three experiments shown in Fig. 15. Figure 16 shows the crack surface in pure iron. It consists of two clearly separated surface morphologies: (1) that of a typical cleavage crack (left part of the figure), and (2) that of a typical ductile fracture (right part of the figure). The first, i.e. the cleavage cracking, has occurred during the void collapse experiment under pure compression,

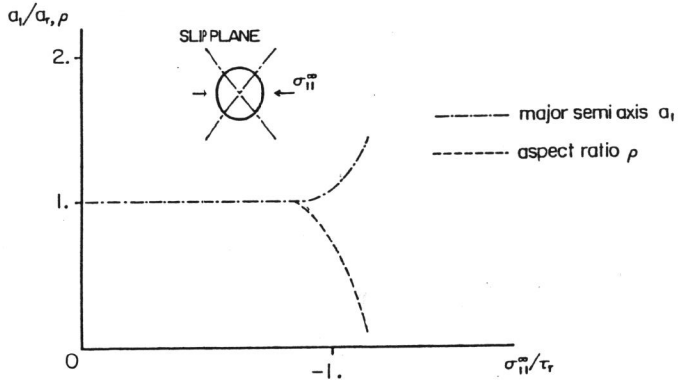

Fig. 13. Change of aspect ratio ρ and major semi-axis a_1 under uni-axial compression $\dot{\sigma}_{11}^{\infty}/\tau_r = -10^2/s$ (from Nemat-Nasser and Hori, 1987).

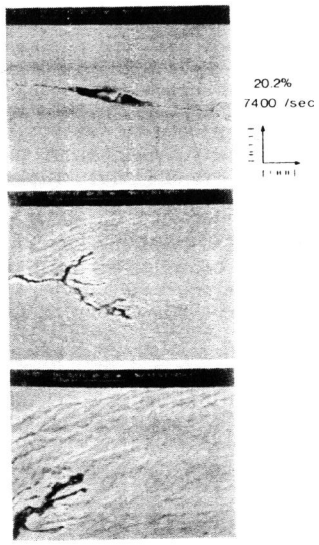

Fig. 14. Void collapse and subsequent tensile cracking under uni-axial compression in single crystal copper (experiment by Dr. Soon-Nam Chang).

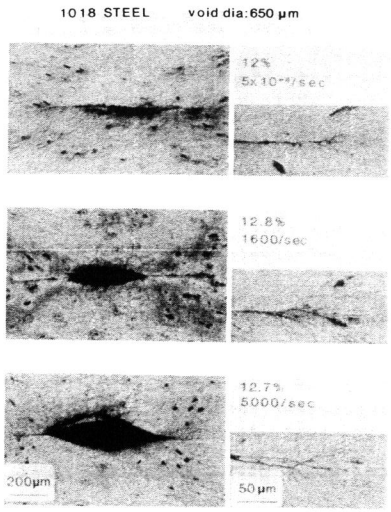

Fig. 15. Void collapse and subsequent tensile cracking under uni-axial compression in 1018 steel.

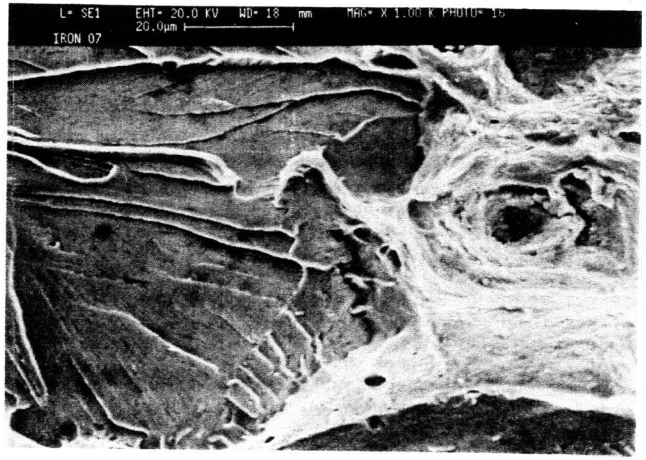

Fig. 16. Surface morphologies of brittle cracking formed normal to applied compression (left) and ductile cracking formed normal to tension (right); (experiment by Mr. Jason Schwartz).

whereas the second, i.e. the ductile cracking, occurred *after* the experiment had been completed and while the cracked sample was being pulled apart in order to expose the crack surface to observation. It is most interesting to note that the compression-induced tensile cracking in this material is a brittle cleavage crack, whereas further extension of this cleavage crack under applied tension involves ductile fracturing. Thus, the tip of the crack formed in compression normal to the applied compressive stresses is clearly marked by the boundary between the cleavage (brittle) fracture surface and the ductile fracture surface.

It is therefore seen that *brittle-type tensile cracking is produced in very ductile single and polycrystals under purely compressive loads, in a direction normal to the applied compression*. The large local plastic flow during void collapse produces residual strains which, during unloading, create cracks. Since, in the absence of voids, the failure mode of the same material is by ductile rupture, it can be concluded that the compression-induced large plastic flows produce certain embrittlement and hence, change the mode of failure of the material. To completely understand the microstructural changes that result in such a response, detailed studies of the dislocation structure in the region close to the collapsed void are required. For detailed discussion and additional experimental results the reader is referred to Nemat-Nasser and Chang (1988).

ACKNOWLEDGEMENT

This work has been supported in part by the National Science Foundation under grant No. MSM-86-15361 and in part by the U.S. Army Research Office under Contract No. DAAL-03-86-K-0169, to the University of California, San Diego.

REFERENCES

Ashby, M. F. and S. D. Hallum (1986). The failure of brittle solids containing small cracks under compressive stress states. *Acta Metall.*, 34, 497-510.

Brace, W. F. and E. G. Bombolakis (1963). A note on brittle crack growth in compression. *J. Geophys. Res.*, 68, 3709-3713.

Bridgman, P. W. (1931). *The Physics of High Pressure*. Bell, London.

Donath, F. A., R. T. Faill and D. G. Tobin (1971). Deformational mode fields in experimentally deformed rock. *Bull. Geol. Soc. Am.*, 82, 1441-1461.

Dugdale, D. S. (1960). Yielding on steel sheets containing slits. *J. Mech. Phys. Solids*, 8, 100-104.

Fairhurst, C. and N. G. W. Cook (1966). The phenomenon of rock splitting parallel to the direction of maximum compression in the neighbourhood of a surface. *Proc. 1st Cong. Int. Soc. Rock Mech., Lisbon*, 1, 687-692.

Hallbauer, D. K., H. Wagner and N. G. W. Cook (1973). Some observations concerning the microscopic and mechanical behaviour of quartzite specimens in stiff, triaxial compression tests. *Int. J. Rock Mech. Min. Sci. Geomech. Abstr.*, 10, 713-726.

Hoek, E. and Z. T. Bieniawski (1965). Brittle fracture propagation in rock under compression. *Int. J. Fract. Mech.*, 1, 137-155.

Holzhausen, G. R. (1978). Sheet structure in rock and some related problems in rock mechanics. Ph.D. thesis, Stanford University, Stanford, California.

Holzhausen, G. R. and A. M. Johnson (1979). Analyses of longitudinal splitting of uniaxially compressed rock cylinders. *Int. J. Rock Mech. Min. Sci. Geomech. Abstr.*, 16, 163-177.

Horii, H. and S. Nemat-Nasser (1983). Estimate of stress intensity factors for interacting cracks. In *Advances in aerospace, structures, materials and dynamics* (U. Yuceoglu, R. L. Sierakowski & D. A. Glasgow, eds.), Vol. AD-06, pp. 111-117. New York: ASME.

Horii, H. and S. Nemat-Nasser (1985). Compression induced microcrack growth in brittle solids: Axial splitting and shear failure. *J. Geophys. Res.*, 90, 3105-3125.

Horii, H. and S. Nemat-Nasser (1986). Brittle failure in compression: Splitting, faulting, and brittle-ductile transition. *Trans. of Roy. Soc. London*, 319, 337-374.

Jaeger, J. C. and N. G. W. Cook (1963). Pinching-off and disking of rocks. *J. Geophys. Res.*, 68, 1759-1765.

Janach, W. (1977). Failure of granite under compression, *Int. J. Rock Mech. Min. Sci. Geomech. Abstr.*, 14, 209-215.

Kirby, S. H. and A. K. Kronenberg (1984). Deformation of clinopyroxenite: Evidence for a transition in flow mechanisms and semibrittle behaviour. *J. Geophys. Res.*, 89, 3177-3192.

Mogi, K. (1966). Pressure dependence of rock strength and transition from brittle fracture to ductile flow. *Bull. Earthq. Res. Inst.*, 44, 215-232.

Nemat-Nasser, S. and H. Horii (1982). Compression-induced nonplanar crack extension with application to splitting, exfoliation, and rockburst. *J. Geophys. Res.*, 87, 6805-6821.

Nemat-Nasser, S. and M. Hori (1987). Void collapse and void growth in crystalline solids. *J. Appl. Phys.*, 62, 2746-2757.

Nemat-Nasser, S. and M. Obata (1988). A microcrack model of dilatancy in brittle materials. *J. Appl. Mech.*, 55, 24-35.

Nemat-Nasser, S. and S.-N. Chang (1988). Compression-induced void collapse and tensile cracking in ductile single and polycrystals. (in preparation).

Olsson, W. A. and S. S. Peng (1976). Microcrack nucleation in marble. *Int. J. Rock Mech. Min. Sci. Geomech. Abstr.*, 13, 53-59.

Scholtz, C. H., G. Boitnott and S. Nemat-Nasser (1986). The Bridgman ring paradox revisited. *PAGEOPH*, 124, 587-599.

Steif, P. S. (1984). Crack extension under compressive loading. *Engng. Fract. Mech.*, 20, 463-473.

Tobin, D. G. and F. A. Donath (1971). Microscopic criteria for defining deformational modes in rock. *Bull. Geol. Soc. Am.*, 82, 1463-1476.

Tullis, J. and R. A. Yund (1977). Experimental deformation of dry Westerly granite. *J. Geophys. Res.*, 82, 5705-5718.

Wong, T. F. (1982). Micromechanics of faulting in Westerly granite. *Int. J. Rock Mech. Min. Sci. Geomech. Abstr.*, 19, 49-64.

Zheng, Z., N. G. W. Cook, F. M. Doyle and L. R. Myer (1988). Preservation of stress-induced microstructures in rock specimens. Report, Lawrence Berkeley Laboratory, University of California, Berkeley, 1-14.